High Performance Amorphous Silicon Image Sensor for X-ray Diagnostic Medical Imaging Applications

Richard L. Weisfield*, Mark Hartney, Roger Schneider, Koorosh Aflatooni, Rene Lujan

dpiX, LLC, Palo Alto, CA 94304

ABSTRACT

Following our previous report[1] concerning the development of a 127 μm resolution, 7.4 million pixel, 30 x 40 cm^2 active area, flat panel amorphous Silicon (a-Si) x-ray image sensor, this paper describes enhancements in image sensor performance in the areas of image lag, linearity, sensitivity, and electronic noise. New process improvements in fabricating a-Si thin film transistor (TFT)/photodiode arrays have reduced first-frame image lag to less than 2%, and uniformity in photoresponse to < 5% over the entire 30 x 40 cm^2 active area. Detailed analysis of image lag vs. time and x-ray dose will be discussed. An improved charge amplifier has been introduced to suppress image cross-talk artifacts caused by charge amplifier saturation, and system linearity has been optimized to eliminate banding effects among charge amplifiers. Preliminary sensitivity improvements through the deposition of CsI(Tl) directly on the arrays are reported, as well as overall imaging characteristics of this improved image sensor.

Keywords: a-Si, TFT, photodiode, imager, sensor, x-ray, array

1. INTRODUCTION

Large-area flat panel amorphous-silicon based image sensors have recently been developed for x-ray imaging applications.[1-7] Such imagers can provide low cost, high resolution, and high dynamic range. Using similar TFT technology to that used in making active matrix liquid crystal displays (AMLCDs), an array of low leakage-current TFT switches can be used to accumulate and store charge in each pixel and then read out each pixel one row at a time. Different means of converting x-ray images into electronic signals have been used or proposed, including thick photoconductors such as Selenium[4-6] and Lead Iodide[7], and thinner a-Si photodiodes[1-3] which sense visible light produced by Gd_2O_2S:Tb phosphor screens or CsI(Tl) scintillating layers. The latter form of image sensor, using *nip* photodiodes and TFT switches, is the subject of this paper.

In a previous paper[1], we described preliminary results on a large-area image sensor with 127 μm pixels using this TFT/photodiode technology. The sensor array is made on a single glass substrate and has an active area of approximately 30 x 40 cm^2 . It uses specially designed gate drivers and readout amplifers which are connected to the array using tape-automated bonding (TAB), similar to the packaging technology used in AMLCDs. The sensor is housed inside a low profile enclosure which contains the array module, analog-to-digital converters, power regulators, and control logic. The sensor is connected to a digital frame grabber card which sits inside a PC, and can read an image of 7,372,800 pixels every 3.2 seconds. Software installed inside the PC is used to correct each pixel for gain and offset variations, as well as correct for isolated bad pixels.

This paper describes improvements made to the large-area image sensor, both in the areas of array technology and in system design. Specifically, we have characterized the transient behavior of the sensor after exposure to varying degrees of x-ray exposure, and have been able to reduce image ghosting artifacts by a factor of four. We also uncovered an intrachip crosstalk phenomemon which occurs when the image sensor is highly exposed and the readout amplifiers are saturated. This crosstalk phenomenon has been

* Correspondence: Email: weisfield@dpix.com; Telephone: 650 842 9644; Fax: 650 842 9808

analyzed and a new readout amplifier has been developed which eliminates this problem. We also show conditions in which gain and offset corrections alone are insufficient for producing a uniform image. By reducing nonuniformities in amplifier linearity, we are able to demonstrate highly uniform flat-field images. Finally, improvements in x-ray sensitivity by incorporating a carbon fiber cover and a CsI scintillator and reductions in electronic noise have also been achieved.

2. ARRAY TRANSIENT BEHAVIOR

One aspect of image sensor performance which has grown in prominence is transient behavior, particularly the decay or lag in an image signal after x-ray exposure. Early prototype systems had first-frame image lag of 10% or less over most of the substrate area for x-ray doses which do not saturate the charge capacity of the photodiode. In applications such as fluoroscopy, where relatively low dose imaging is performed, image lag is relatively insignificant. In fact, some degree of image lag, say < 10%, is considered to be useful, since it provides an analog form of recursive filtering.[4] Similarly, in many medical imaging applications in which contrast is not especially high and doses are kept low, image lag is not usually a problem.

However, we have encountered situations where image lag is an issue, namely, in image calibration, high contrast imaging, and transitions from high dose to low dose imaging. In order to minimize the effects of noise in the calibration process, it is beneficial to average the dark and flat-field images used to provide offset and gain coefficients for each pixel. Repetitive acquisition of stable images is predicated on the assumption that images do not drift significantly between acquisitions. For dark images, one can wait until the imager has warmed up and stabilized in order to obtain stable dark images, and so offset images have always been acquired in an averaging mode. However, if incomplete charge transfer and sufficient charge trapping occur, then as soon as the sensor is exposed to x-ray exposures, there will be a difference in response between the first flat-field exposure and subsequent exposures. Early systems showed about a 12% reduction in signal between the first-frame exposure signal and steady-state levels. This degree of variation makes it impractical to perform multi-frame averaging of flat-field images, so the quantum noise in the flat-field image will add to the overall noise in the corrected images.

A second area where image lag is important is in high contrast imaging. This is not necessarily such a problem in medical imaging, but is more noticeable in nondestructive imaging applications where one is interested in x-raying a very dense object. In this situation, a rather large dose may be used to penetrate the object and the unattenuated x-rays surrounding the object highly expose the image sensor. If another image is taken soon afterwards, the residual image from the areas of overexposure cause a “ghost” image, which can interfere with the evaluation of the image. We have undertaken efforts to understand and minimize this ghosting effect by reducing charge trapping in the photodiode, as shown in a series of images in Figure 1, 2, and 3.

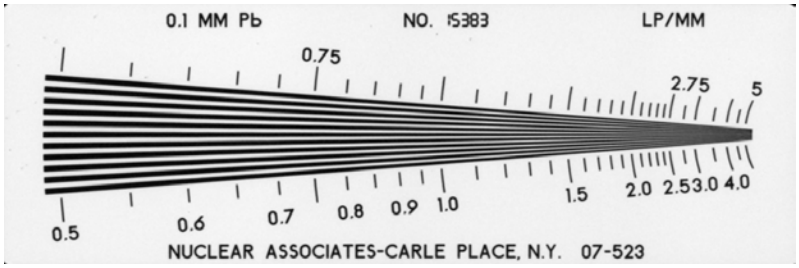

Figure 1. Radiographic image of a high contrast, resolution target taken at 77 kVp, 2.5 mAs. Initial signal level equals 3.4 Me.

In Figure 1 we show a radiographic image of a high contrast, resolution target, taken at a 2.5 mAs, 77 kVp dose which produces approximately 3.4 Me of charge per pixel in unattenuated areas. In Figure 2 we show an image taken 10 seconds after x-ray exposure on an early prototype system, with the image

contrast window increased 10X in order to better reveal the ghost image. The residual charge per pixel is approximately 2.5% of the level in the initial radiograph. In Figure 3, we show an image taken with a recent, improved array exposed under identical conditions, which shows a 4X reduction in image lag to 0.6%. With these improvements, the imager can now perform multiframe averaging, which reduces noise in corrected images by 25%, since the quantum noise in the calibration data can be effectively averaged out. The improved imager can also take multiple radiographs now with minimal ghosting.

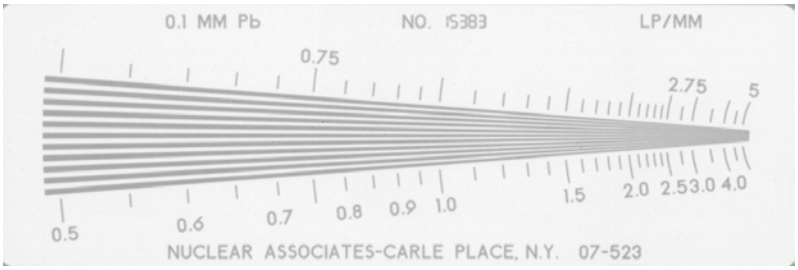

Figure 2. Ghost image taken 10 seconds after radiograph on prototype imager.
Image window decreased 10 x. Residual signal equals 90 ke (2.5 % of initial signal).

Figure 3. Ghost image taken 10 seconds after radiograph on improved imager with reduced level of traps.
Image window decreased 10 x. Residual signal equals 20 ke (0.6 % of initial signal).

A comparison of the way the prototype array images and current, lower-trap-density array images decay with time is shown in Figure 4.

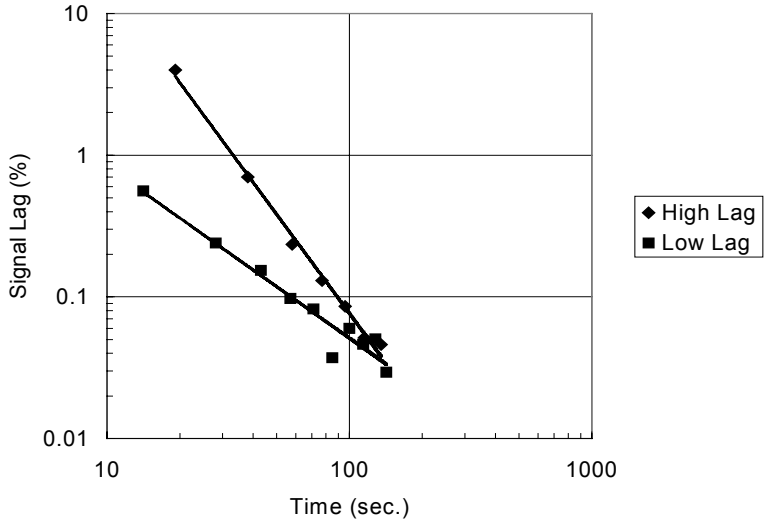

Figure 4. Comparison in signal lag after x-ray exposure for a prototype imager with higher lag and an improved imager
with reduced defect density and lower lag.

Both images show decays which fall off linearly on a log-log scale. The array with higher initial lag falls off much more rapidly with time that the arrays with the lower initial lag: after approximately 100 seconds the ghost images are about indistinguishable. As a result of process modifications intended to reduce defects in the a-Si photodiodes, we interpret these differences in decay as due to reductions in charge trapping within the photodiode. Even in the case of the reduced lag array, it is clear that it takes hundreds of seconds for the imager to return to complete equilibrium. This is expected to cause a problem in situations where a low dose image, such as a fluoroscopy sequence, is taken soon after a high dose radiographic image. While the image sensor we describe in this paper is not designed to operate under fluoroscopic operation, we have used this imager in radiographic mode to measure image lag as a function of different operating conditions over times up to 1000 secs. With this understanding, we will propose a simple algorithm for correcting fluoroscopic images which take into account the time-dependent ghost image produced by a prior radiographic image.

The phenomenon of image lag is shown quantitatively in Figure 5 using a recently produced imager made under improved processing conditions which minimize charge trapping states in the a-Si photodiode.

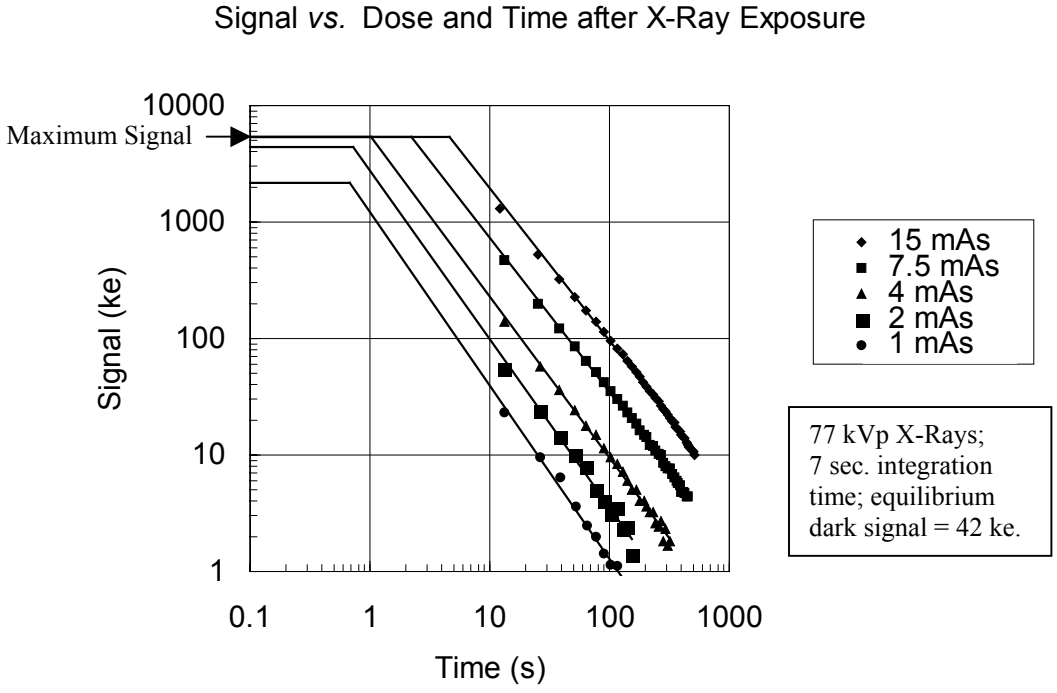

Figure 5. Signals measured with 7 sec. frame times during and following different x-ray exposures. The charge decays can be used to determine excess leakage currents *vs.* time, which can in turn be extrapolated to short integration times, such as used in real-time fluoroscopy.

This data set shows the average signal (with the dark offset subtracted off) *vs.* time for different levels of x-ray exposure. Before each x-ray exposure the sensor was operated in the dark for approximately 20 minutes to restore the traps to their equilibrium state. The integration time per frame was approximately 7 seconds, which provides extremely high sensitivity to transient leakage currents. Each ADC level is approximately 1400 e, so a 7 sec.frame time corresponds to a sensitivity of 0.032 fA per

ADC level. The noise in our measurements in these averaged signals is about ±0.3 ADC units, so the noise in terms of leakage current is about 0.01 fA. Since the equilibrium dark leakage current is typically 1 fA per pixel, this allows us to measure differences from equilibrium down to about 1%.

The most striking characteristic of these decay curves is that the decays all fall on linear and nearly parallel lines on a log-log plot, meaning that $I(t) \sim I_0 t^{\alpha}$, where the exponent α is nearly identical over a wide range of exposure conditions. Such algebraic decays are characteristic of charge trapping and emission from a continuous distribution of deep states, which is a well known property of amorphous semiconductors such as a-Si.[10]

What is less clear from Figure 5 is that the amount of lag at a specific time after the x-ray exposure is not a constant fraction of the x-ray dose as the dose increases, since the maximum signal we can measure during these tests was limited to rather small doses. However, by extrapolating how much signal charge is produced in the initial x-ray exposure, we replot the data as the percentage of image lag *vs.* time in F

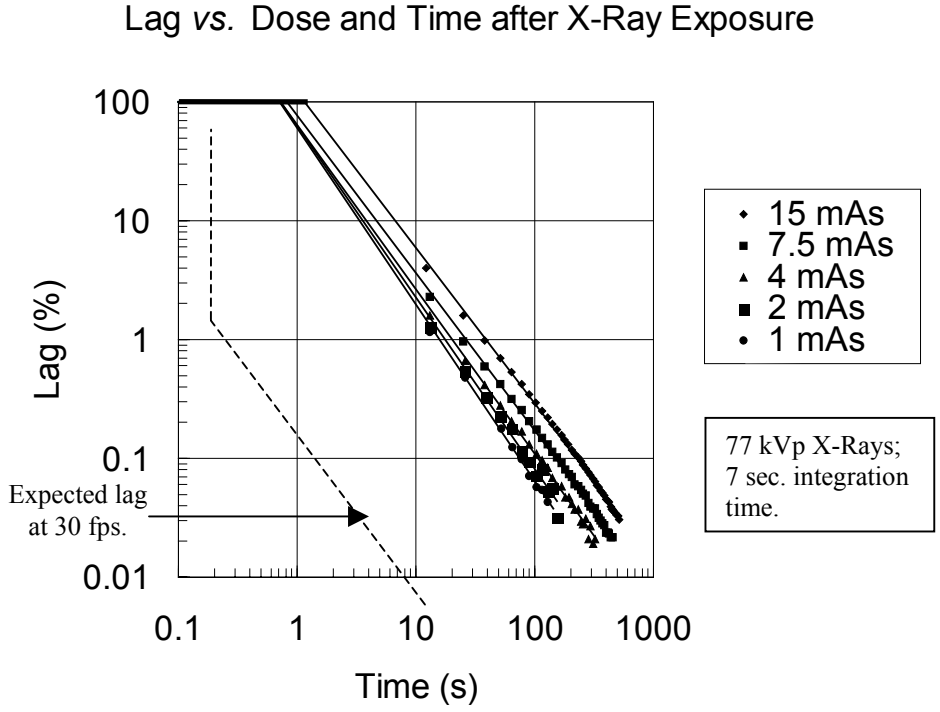

Figure 6. Percentage lag, defined as measured signal / initial signal * 100 %, *vs.* time for different level of x-ray exposure. These lag data are taken for 7 sec. frame times. The extrapolated lag for 30 fps fluoroscopy taken after a 10 mAs radiographic exposure is shown as the dashed line.

In this case, image lag is defined as Lag = measured signal / initial signal * 100 %. Again, the lag transients all show parallel algebraic curves. The other interesting point to note is that the degree of lag starts out at about 1% for small x-ray exposures and increase to over 4% by the time the x-ray exposure is raised to 15 mAs. It turns out that at this dose, the extrapolated initial x-ray signal is calculated to be 22 Me, which is greater than 90% of the saturated charge level of the photodiode (C_{PD} * Vbias). At such large x-ray exposures, the lag increases rapidly with exposure, because the photodiode is no longer fully depleted and it takes a long time for internal charge equilibrium to become reestablished.

Another way of understanding the image lag is through measuring its dependence on the bias across the photodiode. In Figure 7 we plot the first-frame lag (taken approximately 5 seconds after a constant x-ray exposure) as a function of the total voltage across the photodiode. We superimpose a fitting function which takes the form L_0 * k ^Vbias + L_∞, where L_0=33%, k=1.9, and L_∞=1%. This data show that

for large negative applied bias voltages, the first-frame lag drops to a level of about 1%, which is basically limited by the charge transfer efficiency of the TFT. We allow for about 4-5 time constants for the transfer of charge from the photodiode to the dataline, so a 99% charge transfer efficiency is expected. With zero applied field the lag is as large as 33%, which indicates the built-in depletion thickness of the diode extends across approximately 67% of the 1.5 μm thick photodiode. Under normal operating conditions, we apply about -5.5 V across the photodiode, so that the typical first-frame lag is less than 2%. This is a compromise between minimizing lag by increasing Vbias and minimizing pixel leakage currents and gate voltage swing across the TFT by decreasing Vbias.

Because the lag has such a well-defined algebraic decay mechanism, we propose a correction method for switching between high dose radiographs and low dose fluoroscopy sequences, which may be superior to measuring an offset image between each pulsed fluoro frame.[5] The idea is that immediately after a radiograph is taken one captures a single image without illumination, which will contain the lag information for each pixel. This frame should be taken two or three frames after the initial exposure so that complete TFT charge transfer can be assumed. It is expected that this lag will decay according to a universal rate corresponding to the function $I(t) \sim I_0 t^{\alpha}$, which can be determined during the calibration of the image sensor. For each subsequent frame, the level of image lag can be extrapolated with this formula and subtracted from the images taken under fluoroscopic doses.

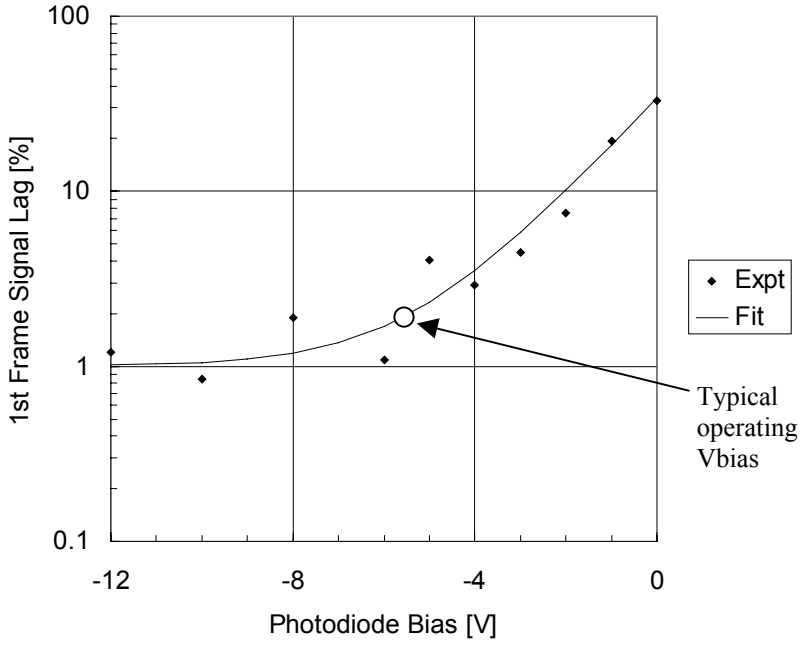

Figure 7. First-frame signal lag as a function of bias voltage applied across the photodiode. The experimental data are fit to the following expression: %Lag = 1% + 33% * 1.9 ^ Vbias.

What is the level of error this methodology introduces? In fluoroscopy, the imager is expected to operate under exposure levels which are 100 to 1000 levels less intense than those used in taking a radiograph. Let us say that we would like to use a continuous x-ray dose of 1 μR/frame at 30 frames per second, which for this pixel size corresponds to 2000 e per pixel, and determine what is the likely error in using this correction method. Let's assume that we take a radiograph at a dose of 10 mAs, where the unattenuated signal would be around 20 Me per pixel. According to figures 5 and 6, at approximately 1 second, we just begin to see the signal decay , using a 7 second integration time. This means that the excess current is approximately 20 Me = 3.2 pC / 7 sec. = 460 fA per pixel at one second after the x-ray exposure. However, using an integration time of 30 frames per second, the integrated charge is much less, corresponding to 460 fA * (1/30) sec = 15 fC = 94 ke. From this time onward we would like to correct for changing image lag. This initial excess charge is almost 50 times larger than the expected magnitude of the

fluoroscopic signal, and its decay will present a significant error. However, if one calculates and subtracts off this lag signal with better than 1% accuracy, the background leakage currents induced by the radiographic exposure should affect the fluoroscopic image with errors which are initially, at one second after x-ray exposure, less than 50% in error. After a few seconds, the errors will fall well below the image noise level. Since this correction method only needs the storage of a single pre-fluoro dark image in memory and a single t^{α} calculation per frame, such corrections can be achieved without significant computational burden. Future work is planned to demonstrate the effectiveness of this approach.

3. IMAGE CROSSTALK

An unexpected artifact of high x-ray exposure that we uncovered in our early prototype systems was a unique form of image crosstalk. The phenomenon is illustrated in Figure 8 (a), where a radiograph of a skull phantom is taken at a dose which saturates the sensor in the unattenuated regions of the image. The

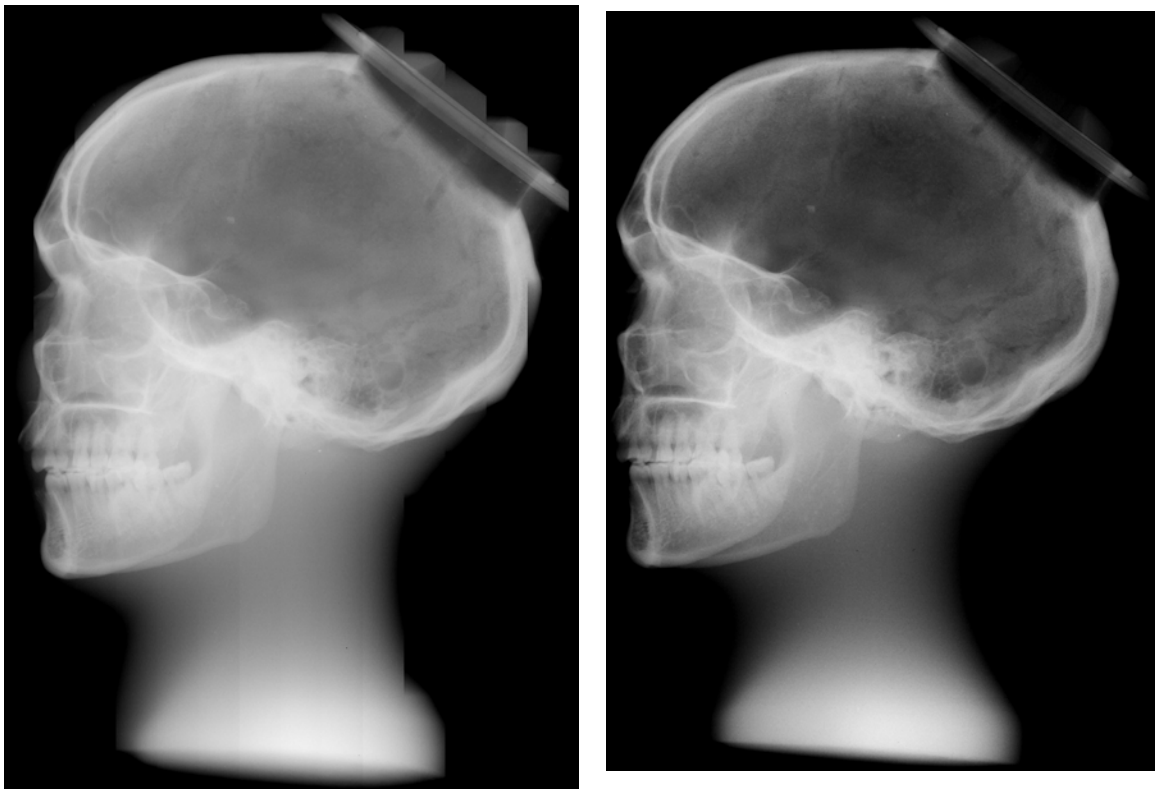

Figure 8. Images of skull phantom image taken near charge amplifier saturation limit at 77 kVp, 5 mAs.
(a) Crosstalk evident at readout chip boundaries. (b) No crosstalk evident in improved imager.

crosstalk shows up as areas where saturated signal levels within a readout chip affect the attenuated signals within the same chip. This causes bands of grey level changes at chip boundaries, making it difficult to image the exact boundaries of objects. We analyze the phenomenon in Figure 9, where we plot the average signal across a row of pixels partially blocked by a piece of lead. The figure shows the signals from four readout chips, each chip containing 128 charge amplifiers connected to corresponding datalines on the array. On the left side of the figure, the imager is not blocked by lead, and the signals from the first two readout chips are saturated (values equal 0). On the right side of the figure, the imager is blocked by lead, and the image values are closer to their dark values. However, the lead object was placed across the middle of the third readout chip's data lines, so that half of its amplifiers were saturated and half received attenuated signals due to the presence of the lead. There are several hundred ADC levels of deviation in the attenuated signals in the third chip compared to the fourth readout chip, where all the amplifiers

received attenuated signals. A dotted line showing what the expected charge inputs should look like is superimposed on the actual image data.

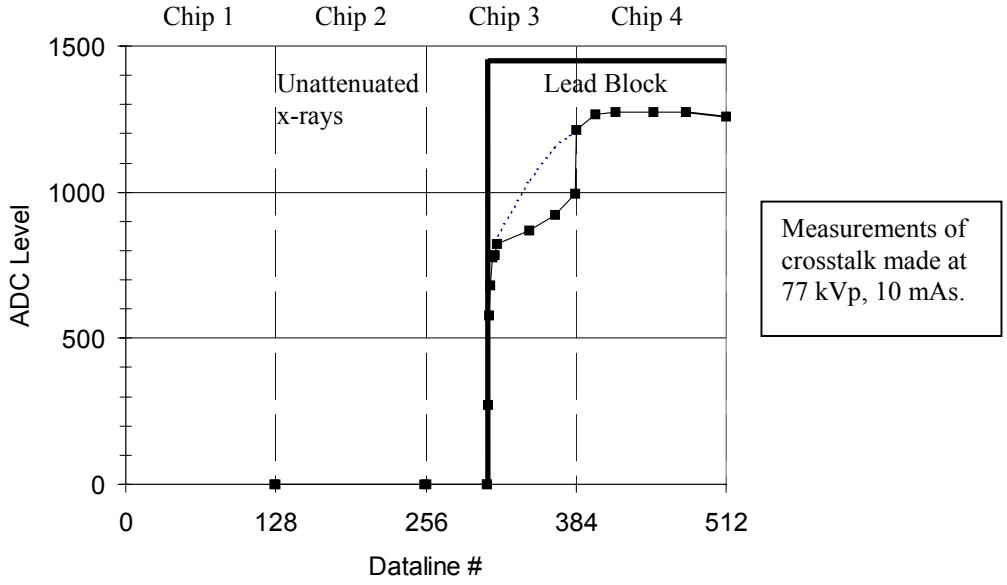

Figure 9. Average signal across a row of pixels partially blocked by a piece of lead. On the left side of the figure are shown the saturated values from the first two readout chips (datalines 0 to 255). On the right side of the figure are shown the ADC levels where the imager is blocked by lead. Where the lead object crosses the middle of the third readout chip's data lines, half the amplifiers are saturated and half receive attenuated signals due to the presence of the lead. There are several hundred ADC levels of deviation in the attenuated signals in the third chip compared to the expected charge levels inferred from lower dose exposures, which are shown as a dotted line superimposed on the actual image data.

This crosstalk phenomenon can be suppressed by reducing the maximum charge levels that the readout amplifiers see. This can be done by reducing the bias voltage on the photodiodes to a level where the saturated charge does not exceed the maximum capacity of the readout amplifier. This reduces the maximum crosstalk significantly, but has two major drawbacks. First, the overall dynamic range and sensitivity of the sensor is reduced. Second, image lag and ghosting effects increase dramatically, as demonstrated in the bias dependence of image lag shown in Figure 7. Of course, in many medical applications, the maximum x-ray dose is limited, so that the charge levels attained do not cause crosstalk. However, it was decided that a more robust solution was needed.

A better resolution to this problem was found in fixing its root cause inside the readout amplifier. We determined that under high levels of signal saturation the internal supply voltage within the readout amplifier decreases, causing all the signal outputs to correspondingly change. The design of the readout chip has now been modified so that its internal supply voltage is no longer sensitive to changes in signal levels. The resultant image of a skull phantom is shown in Figure 8 (b) side by side with the original image which showed crosstalk. We have conducted tests of the new imager for doses up to 100 mAs and find no detectable levels of crosstalk over the entire signal range.

4. IMAGE NONUNIFORMITY

In the process of introducing a redesigned readout chip, we encountered another issue, namely nonuniform flat-field images. The normal procedure for image correction utilizes at least two calibration images: a dark-field image and an image taken under an x-ray exposure close to saturation. All subsequent images are gain and offset corrected using the information from these calibration images. To demonstrate

the uniformity of the imager, a mid-level exposure is taken and the corrected image should appear extremely uniform. However, initial mid-field images taken with the new imager showed significant banding, as shown in Figure 10 (a). The bands represent nonlinearity variations within each readout amplifier, since gain and offset corrections only work properly if the overall imager is uniformly linear in response. We therefore investigated the linearity in response of the redesigned readout amplifier to see if this could be the cause of the nonuniform flat-field images.

To do this we injected known charge pulses into a series of readout amplifiers. The response in ADC level *vs.* input charge is plotted in Figure 11 for several amplifiers within a single readout chip. The curves appear to be very reproducible and quite linear. However, when the derivative of the curve is plotted *vs.* input charge in Figure 12, it is clear that there are two regimes of operation. For small levels of input charge the response shows significant nonlinearity, whereas for larger amounts of negative input charge, the amplifiers are very linear. Attempting to operate the image sensor over the full dynamic range of the readout chip introduces nonlinearities in system response, which result in nonuniformities in the corrected image. We have resolved this problem by injecting charge into each readout amplifier to bias them into their linear range of operation. The resulting flat-field image taken under identical conditions is shown in Figure 10 (b), where all evidence of image banding has been eliminated.

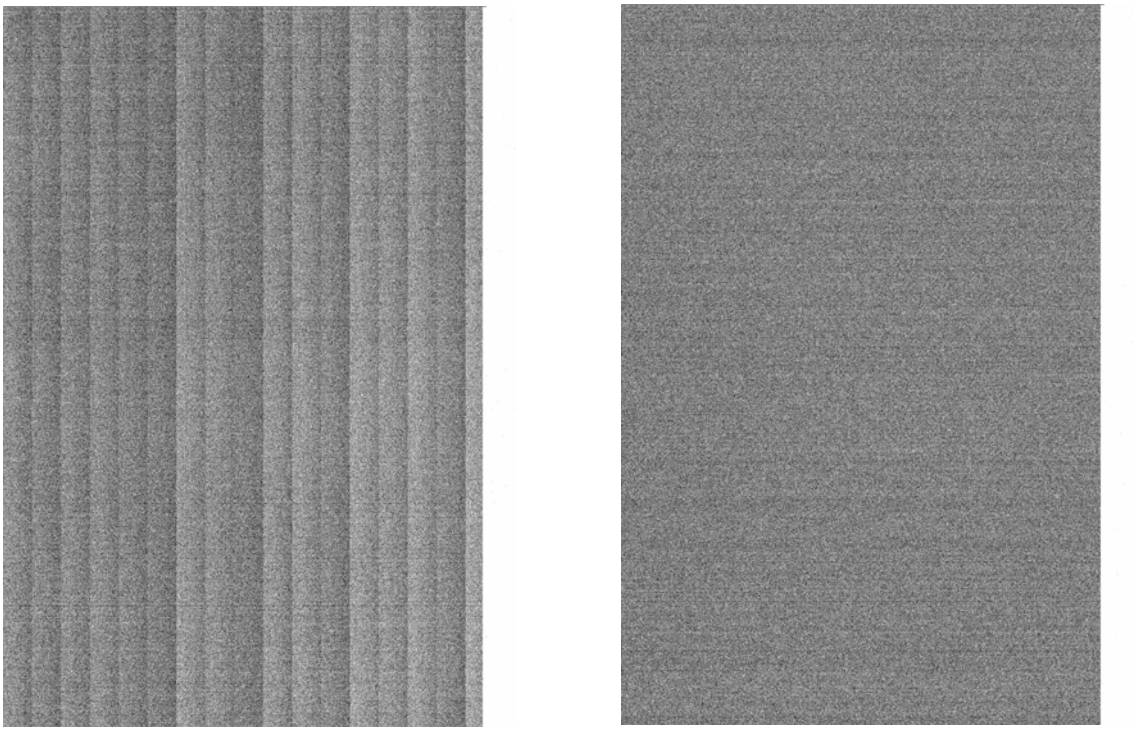

Figure 10. Mid-level, flat-field images (2.5 Me signal levels) shown under a full-scale window of 160 ke.
(a) Gain-compensated image taken without nonlinearity compensation.
(b) Image taken with offset charge injected to compensate for nonuniformity in nonlinearity.

5. SENSITIVITY IMPROVEMENTS

The prototype imagers utilized Kodak Lanex® Regular x-ray phosphor screens, and the imaging module was enclosed in an Aluminum housing. Under these conditions, we measure DQE(0) = 0.25 at 77 kVp. Recent improvements in x-ray sensitivity have recently been introduced. The housing now has a carbon fiber cover which reduces x-ray attenuation, particularly for x-ray energies less than 50 keV. We have also begun developing CsI(Tl) as an x-ray scintillating layer. Preliminary measurements on a 550 µm

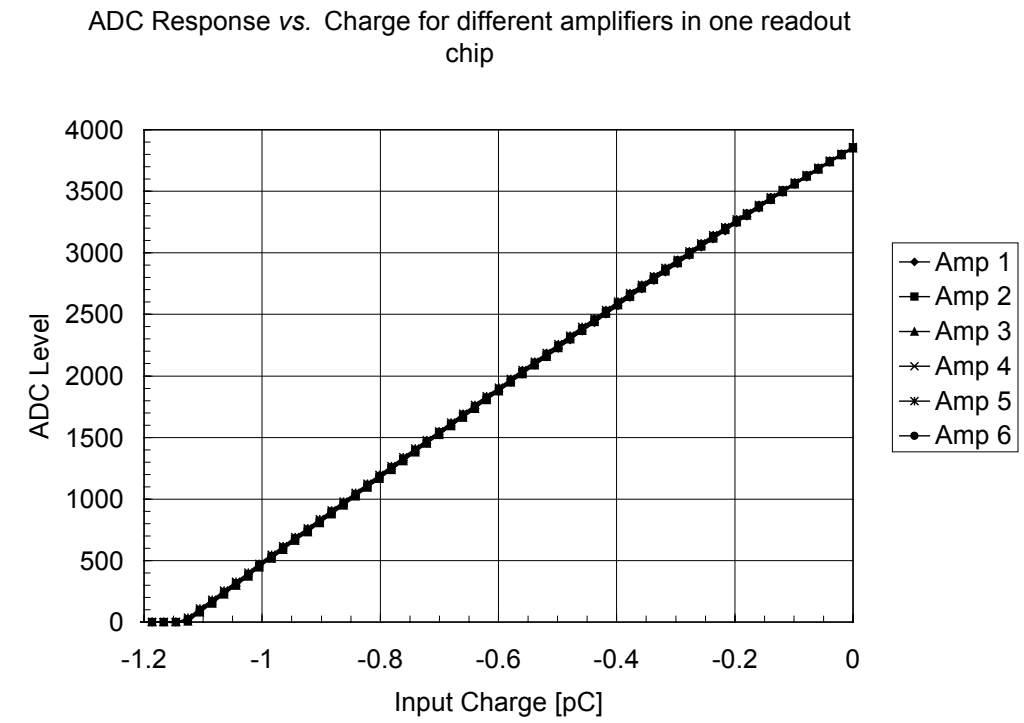

thick layer of CsI(Tl) have yielded sensitivity increases of two to three times that of Lanex® Regular screens, and the DQE(0) has been increased to 0.80 at 77 kVp. The higher DQE(0) agrees with x-ray absorption measurements of 85% made under similar exposure conditions. Optimization of the CsI(Tl) layer to obtain the best compromise between light output, DQE, and MTF are in progress.

Figure 11. The response in ADC level vs. input charge for several amplifiers within one readout chip.

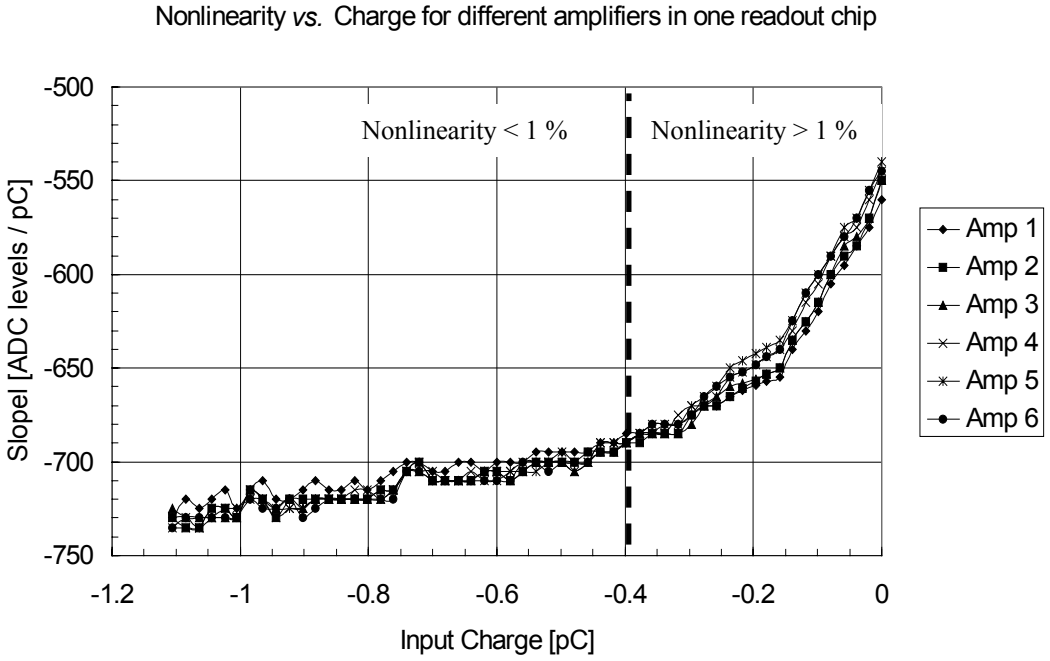

Figure 12. The derivative of the ADC response plotted *vs.* input charge. The nonlinearity in charge amplifier response can be reduced by injecting approximately –0.4 pC of offset charge into each amplifier.

In the area of system electronics, improvements have been made in the analog design which have reduced the electronic noise by nearly a factor of two to 1,600 e per pixel, compared to the 2,500 e noise level achieved in preliminary, prototype systems. These improvements in sensitivity and noise are all expected to provide significant improvements in x-ray image quality, particularly in future, low dose applications.

6. CONCLUSIONS

We have characterized the transient behavior of the sensor after exposure to varying degrees of x-rays, and have been able to reduce image ghosting artifacts by a factor of four. We also uncovered an intrachip crosstalk phenomenon which occurs when the image sensor is highly exposed and the readout amplifiers are saturated. This crosstalk phenomenon has been analyzed and a new readout amplifier has been developed which eliminates this problem. We also show conditions in which gain and offset corrections alone are insufficient for producing a uniform image. By reducing nonuniformities in amplifier linearity, we are able to demonstrate highly uniform flat-field images. Finally, improvements in x-ray sensitivity by incorporating a carbon fiber cover, a CsI(Tl) scintillator and reduced electronic noise have also been achieved.

REFERENCES

1. R. L. Weisfield, M. A. Hartney, R. A. Street, and R. B. Apte, " New Amorphous-Silicon Image Sensor for X-Ray Diagnostic Medical Imaging Applications", SPIE Vol. **3336**, Medical Imaging 1998, Physics of Medical Imaging, 22-24 February 1998, pp. 444-452.
2. L. E. Antonuk, Y. El-Mohri, A. Hall, K-W Jee, M. Maolinbay, S. C. Nassif, X. Rong, J. H. Siewerdsen, Q. Zhao, and R. L. Weisfield, "A Large-Area, 97 μm Pitch, Indirect-Detection, Active Matrix, Flat-Panel Imager (AMFPI)," SPIE Vol. **3336**, Medical Imaging 1998, Physics of Medical Imaging, 22-24 February 1998, pp. 2-13.
3. T. Ducourant, J. Chabbal, C. Chaussat, M. Michel, T. Peppler, and G. Vieux, Medical Imaging 1999, Physics of Medical Imaging, to be published in these proceedings.
4. R.E. Colbeth, M. J. Allen, D. J. Day, D. L. Gilblom, R. A. Harris, I. D. Job, M. E. Klausmeier-Brown, J. M. Pavkovich, E. J. Seppi, E. G. Shapiro, M. D. Wright, and J. M. Yu, "Flat-panel imaging system for fluoroscopy applications," SPIE Vol. **3336**, Medical Imaging 1998, Physics of Medical Imaging, 22-24 February 1998, pp. 376-387.
5. T. J. C. Bruijns, P. L. Alving, E. L. Baker, R. Bury, A. R. Cowen, N. Jung, H. A. Luijendijk, H. J. Meulenbrugge, and H. J. Stouten, "Technical and clinical results of an experimental Flat Dynamic (digital) X-ray image Detector (FDXD) system with real-time corrections", SPIE Vol. **3336**, Medical Imaging 1998, Physics of Medical Imaging, 22-24 February 1998, pp. 33-44.
6. D. L. Lee, L. W. Cheung, L. S. Jeromin, "A New Digital Detector for Projection Radiography," SPIE Vol. **2432**, Medical Imaging 1995, Physics of Medical Imaging, 26-27 February 1995, pp. 237-249.
7. J. A. Rowlands, W. Zhao, I. Blevis, G. Pang, W. G. Ji, S. Germann, S. O. Kasap, D. Waechter, and Z. Huang, "Flat panel detector for digital radiology using active matrix readout of amorphous selenium," SPIE Vol. **3032**, Medical Imaging 1997, Physics of Medical Imaging, 23-25 February 1997, pp. 97-108.
8. A. Tsukamoto, S. Yamada, T. Tomisaki, M. Tanaka, T. Sakaguchi, H. Asahina, and M. Nishiki, "Development of a selenium-based flat-panel detector for real-time radiography and fluoroscopy," SPIE Vol. **3336**, Medical Imaging 1998, Physics of Medical Imaging, 22-24 February 1998, pp. 388-395.
9. R. A. Street, K. S. Shah, S. E. Ready, R. B. Apte, P. R. Bennett, M. Klugerman, and Yu. Dmitriyev, "Large-area x-ray image sensing using a PbI_2 photoconductor", SPIE Vol. **3336**, Medical Imaging 1998, Physics of Medical Imaging, 22-24 February 1998, pp. 24-32.
10. T. Tiedje and A. Rose, "A Physical Interpretation of Dispersive Transport in Disordered Semiconductors," Sol. St. Comm. **37**, pp. 49-52, 1980.